International Journal of Heat and Technology
Vol. 40, No. 6, December, 2022, pp. 1447-1453
Journal homepage: http://iieta.org/journals/ijht

Identification and Prediction of Thermodynamic Disasters During Deep Coal Mining

Min Li*, Xiankang Cheng

Shanxi Lu'an Environmental Energy Dev. Co., Ltd., Changcun Coal Mine, Changzhi 046000, China

Corresponding Author Email: minerhaoxuelimin@163.com

https://doi.org/10.18280/ijht.400612

Received: 20 August 2022
Accepted: 30 October 2022

Keywords:
deep coal mining, thermodynamic disaster, disaster identification, disaster prediction

ABSTRACT

Researching the methods to identify and predict thermodynamic disasters during deep coal mining is a very important work for the design of mine emergency systems and the decision-making of mine rescue and personnel evacuation, however, existing studies only built static models without evaluating or predicting the development trend of thermodynamic disasters, the research on dynamic modeling methods and rescue decision-making is insufficient, and they generally ignored the mechanism of mutual conversion between fire and gas explosion in deep coal mines. Thus, this paper aims to study the identification and prediction of thermodynamic disasters during deep coal mining. At first, the method for analyzing the thermal field in deep coal mining areas is introduced in detail, and the finite element thermal analysis method is adopted to study the thermodynamic disasters during deep coal mining; then, this paper establishes a thermodynamic disaster prediction model based on the improved Kernel-based Extreme Learning Machine (KELM), and introduces the improved Crow Search Algorithm (CSA) to solve the instability of prediction results caused by artificial selection of model parameters. At last, this paper uses experimental results to verify the validity of the proposed model.

1. INTRODUCTION

Thermodynamic disasters are a major type of disasters during deep coal mining, they are caused by uncontrolled combustion and explosion in coal mines. Thermodynamic disasters are abrupt, quick-developing, and prone to secondary disasters, so the rescue is very difficult. Typical thermodynamic disasters include the spontaneous combustion of coal, fire caused by external causes, gas combustion and explosion, and coal dust explosion, etc. [1-9]. During rescue, due to the thermal effect existing in the deep coal mines, usually, gas and leaked air can form mixed combustible gases. If the ventilation in the mining area is not good enough, the continuous explosion caused by combustion of coal and gas can worsen the disaster and make the situation more complicated [10-16]. Moreover, the propagation of shock waves in complex wind networks can damage the ventilation system, once the decision-making misplays, it might expand and deepen the scope and degree of personnel damage [17-24]. Therefore, researching the identification and prediction methods of thermodynamic disasters during deep coal mining is a very important work for the design of mine emergency systems and the decision-making of mine rescue and personnel evacuation.

To investigate the mechanical effects and characteristics of typical thermodynamic disasters in underground coal mines, Chen et al. [25] analyzed the stress source of coal and surrounding rocks, and the occurrence mechanism, evolution, and mechanical performance of typical thermodynamic disasters. Their research findings show that there are obvious mechanical effects during the evolution and occurrence of typical thermodynamic disasters. For the purpose of reducing the risk of coal-rock dynamic disasters during coal mine production, Ma et al. [26] took the coupling mechanics characteristics of coal and rock produced in Dingji Coal Mine as research object to experiment on the deformation features and variation rules of mechanical parameters of raw coal under multi-field coupling (temperature, gas, and stress), the research outcome suggests that the elastic modulus, peak strain, and peak stress of raw coal samples under the action of thermal-hydraulic-mechanical coupling conform to the same variation law within the test temperature range and all of them decrease linearly as the temperature increases. Zhou et al. [27] pointed out that the coal mine belt fire is a type of fire that develops very rapidly and hard to control, it can easily cause airflow disorder and undermine the ventilation system if not put out quickly, and building fire airflow control systems is a good way to prevent belt fire. The authors took the 5-th belt roadway of Kongzhuang coal mine as the subject to build a geometrical model for this roadway, then, based on a mathematical model of fire smoke flow, they simulated the CO volume fraction, smoke density distribution, air temperature, and pollutant velocity vector in the roadway before and after taking airflow control measures in the software Fluent.

Now there are many research achievements in the evaluation and prediction of thermodynamic disasters of coal mines, but still there are a few defects with them in terms of rescue timeliness, dynamics and limitations; moreover, these existing studies only built static models without evaluating or predicting the development trend of thermodynamic disasters, the research on dynamic modeling methods and rescue decision-making is insufficient, and they generally ignored the mechanism of mutual conversion between fire and gas explosion in deep coal mines. In view of these deficiencies, this paper aims to study the identification and prediction of thermodynamic disasters during deep coal mining. In the second chapter, this paper introduces in detail the method for

analyzing the thermal field in deep coal mining areas, and adopts the the finite element thermal analysis method to study thermodynamic disasters during deep coal mining; in the third chapter, this paper establishes a thermodynamic disaster prediction model based on the improved KELM, and introduces the improved CSA to solve the instability of prediction results caused by artificial selection of model parameters. At last, this paper uses experimental results to verify the validity of the proposed model.

2. THERMAL FIELD IN DEEP COAL MINING AREA

This chapter introduces the method for analyzing thermal field in deep coal mining area, investigates the temperature abnormality in the mining area, adopts finite element thermal analysis to study thermodynamic disasters during deep coal mining based on site survey data, and proposes the method for identifying and predicting thermodynamic disasters.

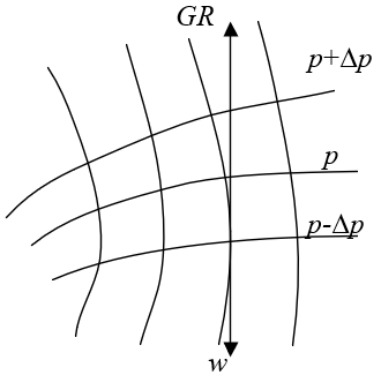

Figure 1. Heat flux density vector in deep coal mining

The heat flux density of thermal field in deep coal mining area refers to the amount of heat transferred within per unit time in unit area of the roadway in deep coal mining area. Figure 1 shows a diagram of the heat flux density vector in deep coal mining. Assuming: w represents the density of heat flow along a certain direction; GR represents the coefficient of thermal conductivity; μ represents the ratio of temperature difference to depth difference, then the following formula gives the Fourier's law:

$$w = -\mu GR \tag{1}$$

where, w and μ are in different directions but they are on the same normal of the isothermal surface; w points to the direction of temperature rise, that is, the heat in the thermal field of deep coal mining area is transmitted from the high temperature zone to the low temperature zone.

For the problem of two-dimensional thermal field in deep coal mining area, isometric line is often used to assist the analysis. In this paper, at first, the temperature gradient method was employed to quantitatively calculate the thermal field temperature in deep coal mining area; then, the Kriging Interpolation was adopted to estimate the temperature data except for the temperature sampling points of site survey, and finally a complete contour map was plotted. The principle is detailed as follows:

Assuming: a is randomly-chosen temperature sampling point in the thermal field of deep coal mining area; $C(a)$ is the temperature value collected at this point; in this mining area, there are a total of m random points a_1, a_2, a_3...a_m; $C(a)$ satisfies the intrinsic hypothesis and second stationary hypothesis within a fixed partition spacing range of the specified mining area, let n represent the mathematical expectation, $d(f)$ represent the covariance function, and $\alpha(f)$ represent the variation function, then there is:

$$\begin{aligned} &O\big(c(a)\big) = n \\ &d(f) = O\big(C(a)C(a+f)\big) - n^2 \\ &\alpha(f) = \frac{1}{2} O\big(C(a) - C(a+f)\big)^2 \end{aligned} \tag{2}$$

On the premise that the hypotheses are met, for the m random temperature sampling points, we can get $C(a_1)$, $C(a_2)$, $C(a_3)$,...,$C(a_m)$, assuming μ represents the weight coefficient, then the following formula gives the estimate of point a_o other than sampling points:

$$C^m(a_0) = \sum_{i=1}^{m} \mu_i C(a_i) \tag{3}$$

Based on the temperature sampling results of site survey and the gradient distribution law of thermal field in deep coal mining area, this paper calculated the roadway temperature in the mining area and the plane temperature distribution at the roadway elevation, so as to analyze the degree of thermodynamic disasters. Assuming: P_f represents the temperature of the calculation point; GR represents the temperature gradient of the calculation point; F represents the burial depth of the calculation point; f represents the depth of the constant temperature layer of the calculation point; P_r represents the temperature of the constant temperature layer of the calculation point, then there is:

$$P_f = \frac{GR(F - f)}{100} + P_r \tag{4}$$

Assuming: F_1 represents the ground elevation of the calculation point, then the formula for calculating P_r is:

$$P_r = -0.004F_1 + 18.3 \tag{5}$$

This paper applied the method of steady-state thermal analysis to the two-dimensional numerical simulation of thermal field distribution in deep coal mining area, and the calculation was performed based on finite element steady state thermal analysis and the conservation law of energy. By default, the sum of the inflow heat of the thermal field system of deep coal mining area W_{in} and the heat of the the thermal field system itself W_{SE} is equal to the outflow heat of the thermal field system W_{out}. At this time, it is considered that the thermal field system of the deep coal mining area is in a thermal stable state and meets the following formula:

$$W_{in} + W_{SE} - W_{out} = 0 \tag{6}$$

When modeling the thermal field distribution in deep coal mining area, the structural shape of roadway and the specific temperature requirement of mining process make the problem more complicated, so conventional analysis methods can

hardly attain the accurate thermal field, while the finite element method can solve this problem. Assuming: σ represents the density of air in the mining area; L_a and L_b represent the thermal conductivity coefficients of air in the mining area along a and b directions of the roadway; W represents the density of heat source; Γ represents the domain of solutions; τ represents the field variable, then the following formula gives the steady state heat conduction equation for the two-dimensional thermal field in deep coal mining area:

$$\frac{\partial}{\partial \delta}\left(l_a \frac{\partial \tau}{\partial a}\right)+\frac{\partial}{\partial b}\left(l_a \frac{\partial \tau}{\partial b}\right)+\sigma w=0\left(\text{within } \Gamma\right) \quad (7)$$

Based on the variational principle, the above formula can be approximately solved by the following formula:

$$\prod(\tau)=\int_{\Omega}\left[\begin{array}{l}\frac{1}{2} l_x\left(\frac{\partial \tau}{\partial a}\right)^2 \\ +\frac{1}{2}\left(\frac{\partial \tau}{\partial b}\right)^2+\sigma W \tau\end{array}\right] d\Omega \quad (8)$$

Based on above formula, after inputting the known thermal physical parameters into the constructed simulation model of thermal field in deep coal mining area, the thermal field in the disaster area can be simulated.

3. THERMODYNAMIC DISASTER PREDICTION MODEL FOR DEEP COAL MINING AREA

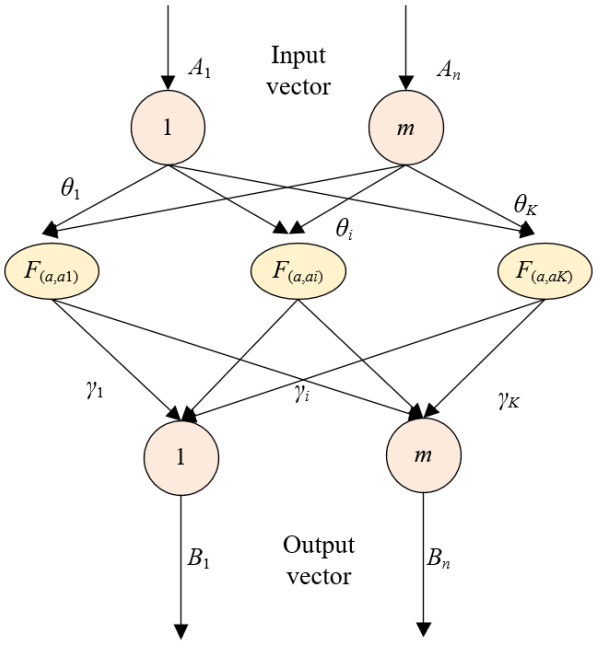

Figure 2. Network structure of KELM

Now coal mining is going down deeper into the ground, the multiple disaster factors such as underground coal and gas, possible ignition sources in the goaf, and ignition characteristics can affect each other, which makes the mining conditions of the site even worse, and the coupling of disaster factors and the ventilation system makes the disaster prediction even more difficult, and the conventional prediction methods can hardly meet the actual requirements of deep coal mining areas. This paper constructed the thermodynamic disaster prediction model based on improved KELM, and introduced the improved CSA to solve the instability of prediction results caused by artificial selection of model parameters.

Compared with the conventional extreme learning machine models, KELM has the merits of less adjustable parameters, stable prediction results, and high prediction efficiency. Figure 2 shows the network structure of KELM. In kernel-based learning methods, the kernel matrix Φ is used to replace the random matrix FF^T in conventional extreme learning machine, which can effectively solve the problem of dimension disaster and reduce the loss of raw data features of multiple influencing factors of the complex disasters, that is:

$$\Phi_{KELM}=FF^T \quad (9)$$

Assuming: (a) represents the output function of the extreme learning machine model; $L(a_i, a_j)$ represents the kernel function, then the activation function $h(a)$ of conventional extreme learning machine can be written in the form of a kernel function as follows:

$$\Phi_{i,j}=f\left(a_i\right) \bullet f\left(a_j\right)=L\left(a_i, a_j\right) \quad (10)$$

To ensure that the characteristic root of FF^T is not zero, the parameter diagonal matrix I and normalized parameter D are introduced into the main diagonal elements of FF^T to determine the weight vector γ*. Through above steps, the prediction stability and generalization performance of the KELM model can be effectively improved. γ* can be transformed by the formula below:

$$\gamma^*=F^T\left(I / D+FF^T\right)^{-1} P \quad (11)$$

Assuming: F represents the hidden layer matrix; F^T represents generalized inverse; $L(a_i, a_j)$ represents the introduced kernel function matrix; P represents the predicted target vector, then the formula below gives the expression of the output function of KELM:

$$\begin{aligned} g(a) &= f(a) F^T\left(\frac{1}{D}+FF^T\right)^{-1} P \\ &= \left[\begin{array}{c} L\left(a, a_1\right) \\ \vdots \\ L\left(a, a_M\right) \end{array}\right]\left(\frac{1}{D}+FF^T\right)^{-1} P \end{aligned} \quad (12)$$

After careful analysis and repeated verification, it is found that for the prediction of thermodynamic disasters in deep coal mining area and such kinds of problems, under the condition of normal numbers of data features and samples, taking the Gaussian radial basis kernel function as the kernel function of the model enables the model to attain better performance in identifying and predicting thermodynamic disasters. Assuming: ε represents the width parameter of the kernel function, by substituting the expression of Gaussian radial basis kernel function into the above formula, the output function could be attained as follows:

$$g(a)=\begin{bmatrix} L(a,a_1) \\ \vdots \\ L(a,a_M) \end{bmatrix}\left(\frac{1}{D}+FF^T\right)^{-1}P$$
$$=\exp\left(-\frac{\|a_i-a_j\|^2}{2\varepsilon^2}\right)\left(\frac{1}{D}+FF^T\right)^{-1}P \quad (13)$$

According to Formula 13, the output value of KELM is determined by D and ε.

4. OPTIMIZATION ALGORITHM FOR THE THERMODYNAMIC DISASTER PREDICTION MODEL OF DEEP COAL MINING AREA

To improve the prediction speed and accuracy of thermodynamic disasters in deep coal mining area, this paper improved the conventional Crow Search Algorithm (CSA) and used it to optimize the KELM, which was then applied to the prediction of thermodynamic disasters in deep coal mining area and effectively prevent the occurrence of such disasters. Figure 3 shows the flow of the improved CSA.

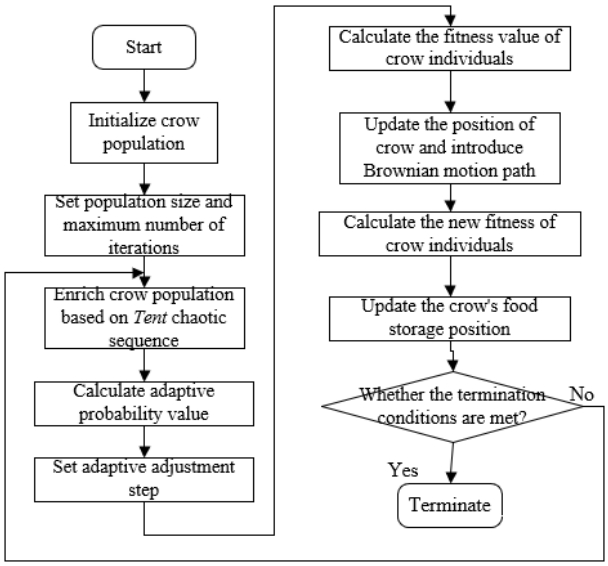

Figure 3. Flow of the improved CSA

To improve the global optimal-searching ability of the algorithm, at first, this paper introduced the *Tent* chaotic sequence into the conventional CSA, that is, to use the randomness of chaotic variable to enrich the diversity of crow population. The expression of the *Tent* chaotic mapping function is given by the following formula:

$$a_{l+1}=\begin{cases} 2a_l, 0\le a_l\le 0.5 \\ 2(1-a_l), 0.5\le a_l\le 1 \end{cases} \quad (14)$$

Assuming: A_m represents the upper limit of each dimension of each crow individual, A_i represents the corresponding lower limit, A represents the crow individual after mapping, then, in order to initialize the crow population, this paper mapped the variable created by the *Tent* mapping to crow individuals based on the following formula:

$$A=A_i+(A_i-A_m)A_{l+1} \quad (15)$$

To overcome the shortcoming of global search and local search imbalance of conventional CSA, this paper introduced a key parameter, the adaptive perception probability, to make sure that the AP value of the crow population won't alternate between high and low suddenly during the iteration process, that is, to stabilize the performance of the algorithm. Assuming: GZ_1 represents the maximum perception probability, GZ_2 represents the minimum perception probability, ϕ_{max} represents the maximum number of iterations, FIT_{max} represents the maximum fitness under current iteration conditions, FIT_{AV} represents the average fitness under current iteration conditions, then the following formula calculates the adaptive perception probability:

$$GZ_{SA}=\begin{cases} \frac{\sqrt{3}(GZ_1-GZ)_2}{\sqrt{0.9\pi}}\exp\left(-\frac{\pi(\varphi)^2}{\varphi_{\max}^2}\right), \\ \qquad FIT_{\max}>FIT_{AV} \\ GZ_1, FIT_{\max}\le FIT_{AV} \end{cases} \quad (16)$$

In order to balance the local searching ability and global optimal searching ability of CSA, this paper introduced the adaptive adjustment step, assuming C represents the distance between leader y and the current individual x, κ represents the scaling factor, then there is:

$$\begin{cases} gk_{SA}=\sqrt{\sum_{l=1}^{c}\left(n_{yl}^p-n_{yl}^p\right)^2}\times\kappa \\ C=\sqrt{\sum_{l=1}^{d}\left(n_{yl}^p-n_{xl}^p\right)^2} \end{cases} \quad (17)$$

In later iterations of the algorithm, the step size was automatically reduced to shorten the distance between the current crow individual and the optimal crow individual, in this way, the local searching ability could be improved and the diversity of crow population could be balanced, then there is:

$$a^{x,\varphi+1}=\begin{cases} a^{x,\varphi}+s_x*gk^{x,\varphi}*\left(n^{y,\varphi}-a^{x,\varphi}\right), \\ \qquad s_y\ge GZ^{x,\varphi} \\ \text{Any position}, s_y<GZ^{x,\varphi} \end{cases} \quad (18)$$

At last, this paper introduced the random motion process, namely the Brownian motion, into conventional CSA. Assuming: variable $Y(p)$ simulates the Brownian motion path on $[0, P]$, $Y(p)$ needs to satisfy three conditions: 1) In the initial state, $Y(0)=0$; 2) For any $p>r$, $Y(p)$-$Y(r)$ is independent of the previous process: $:0\le v\le r$; 3) For any $p>r$, $Y(p)$-$Y(r)\sim M(0, p-r)$. Assuming: a and b represent one-dimensional Brownian motion; when $s_y<GZ^{a,\phi}$, the crow individual y adopts the random search method to confuse tracker x; D represents a constant number; v represents a random number between 0 and 1; RB represents the Brownian motion; T_{best} represents the

optimal position found by crows in the current population, then there is:

$$a^{x,\varphi+1} = a^{x,\varphi} + s_x * gk_{SA} * \left(n^{y,\varphi} - a^{x,\varphi}\right), \quad s_y \geq GZ^{x,\varphi} \tag{19}$$

$$a^{x,\varphi+1} = a^{x,\varphi} + D * \upsilon * RB(x,y) * \left(T_{best} - RB(a,b) * a^{x,\varphi}\right), s_y < GZ^{x,\varphi} \tag{20}$$

5. EXPERIMENTAL RESULTS AND ANALYSIS

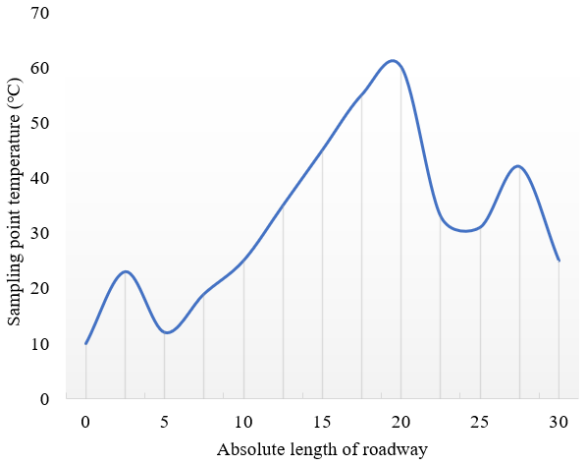

Figure 4. Sampling point temperature distribution in deep coal mining area

Figure 4 shows the distribution of sampling point temperature in the deep coal mining area. According to the figure, the temperature of sampling points in the mining area is mainly affected by the absolute length of the roadway. In the event of a thermodynamic disaster, hot air and smoke would spread along the roadway. To figure out the impact of the absolute length of roadway on the smoke flow at high temperature, the temperature of sampling points in the deep coal mining area was simulated under different absolute lengths of roadway, and the results show that, with the change of the absolute length of roadway, the smoke backflow distance near the center of the disaster area increases, and the sampling point temperature in the deep coal mining area rises with fluctuations.

In this paper, since the thermal field in deep coal mining area is a two-dimensional heat conduction model, for the setting of hypothesis condition of the fixed partition spacing range of mining area, four boundaries were set (upper, lower, left, and right boundary), wherein the left and right boundaries correspond to the inlet and outlet positions of the deep coal mining area. In this paper, it is assumed that the heat in the thermal field system of deep coal mining area does not exchange with the outside, and the upper and boundary conditions were respectively set as the temperate of the constant temperature layer and the predicted temperature of a certain depth. Table 1 gives the temperature values of the deep coal mining area in finite element numerical simulation. Based on the analysis method given in this paper, it is known that the temperature of the constant temperature layer and the depth of roadway have determined the set value of lower boundary temperature. Combining with the temperature data actually measured at the site during survey, the predicted air temperature values of the lower boundary at different ground elevations were calculated. The temperature contour map of the lower boundary of the model can be attained via Kriging interpolation, and the temperature values of the boundary within the range of the next partition spacing could be attained.

Table 1. Temperature of the deep coal mining area during finite element numerical simulation

Ground elevation (*m*)	Upper boundary temperature (℃)	Ground elevation (*m*)	Lower boundary temperature (℃)
2200-2300	9.258	3200-3300	5.263
2300-2400	8.247	3300-3400	5.481
2400-2500	8.263	3400-3500	4.629
2500-2600	8.925	3500-3600	4.325
2600-2700	7.421	3600-3700	3.271
2700-2800	7.629	3700-3800	3.152
2800-2900	7.385	3800-3900	3.928
2900-3000	6.128	3900-4000	2.152
3000-3100	6.352	4100-4200	2.306
3100-3200	5.294	4200-4300	1.274

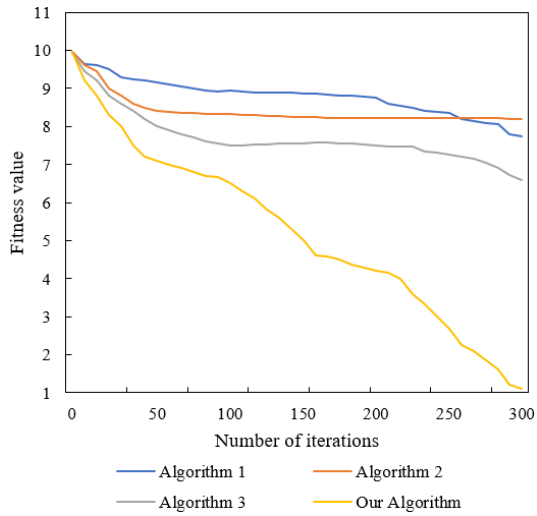

Figure 5. Fitness curves of different optimization algorithms

To verify the validity of the KELM optimized by the improved CSA, we designed experiments to compare the fitness of different optimization algorithms, including the Particle Swarm Optimization (PSO, reference algorithm 1), Artificial Fish School (AFS, reference algorithm 1), and Ant Colony Optimization (ACO, reference algorithm 3). Figure 5 shows the fitness curves of different optimization algorithms. According to the figure, compared with the fitness of other optimization algorithms, the optimal fitness value of the proposed algorithm is more than ten orders of magnitude lower, so the performance of the proposed algorithm in optimal-searching is the best compared with the other three algorithms.

Because the initial weight vector of KELM was selected randomly, as the network training continues, the number of hidden layer neurons of the model changed accordingly, so in order to test the validity and reliability of the output results of the thermodynamic disaster prediction model, 10 groups of experiments were carried out, and the average value of all experimental groups was calculated. Figure 6 compares the average and true values of verification samples and test samples.

Table 2 gives the prediction results of the safety level of thermodynamic disasters in deep coal mining area. According to Table 2, in the 100 test results, only 3 are inconsistent with the real situation. Table 3 gives the incorrect prediction data of safety level of thermodynamic disasters in deep coal mining area.

According to statistical results, the prediction accuracy of the model for the safety level of thermodynamic disasters reached more than 97%. Although there are large errors in the prediction results of a small number of samples during model training, the average value of the prediction results is not much different from the real value, so it can be considered that the predicted thermodynamic disaster in deep coal mining area is the same as the real situation. Therefore, in actual application scenarios, the proposed model needs to be trained a few more times, and the average value of the training results will be output as the final prediction result. According to above experimental results, the prediction performance of the model is stable and has strong generalization ability, the model can be used to predict the thermodynamic disasters in other deep coal mining areas.

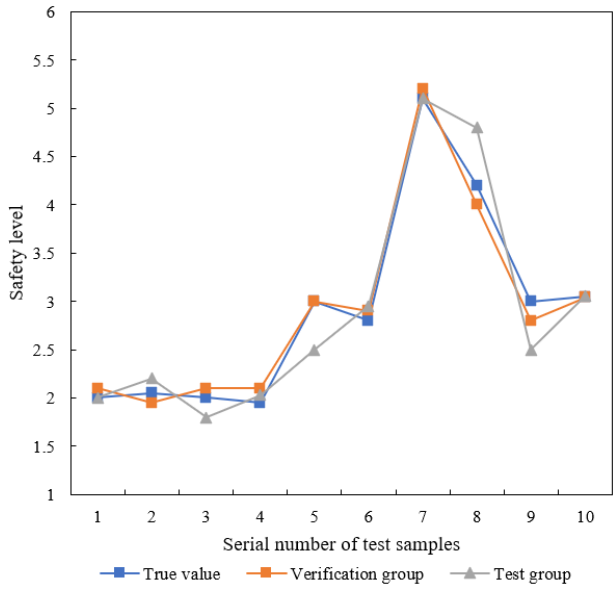

Figure 6. Comparison of verification samples, test samples, and real values

Table 2. Prediction results of the safety level of thermodynamic disasters in deep coal mining area

Sample No.		1#	2#	3#	4#	5#	6#
Real value of safety level		**3**	**3**	**3**	**4**	**4**	**4**
Evaluation result of test sample	Group 1	2.3067	2.4185	2.6158	2.5174	2.0415	3.4172
	Group 2	2.5185	2.9614	2.3958	2.3629	2.6291	2.0369
	Group 3	2.3014	2.0143	2.3514	2.3857	2.3417	2.3417
	Group 4	1.2693	2.6258	2.3025	2.1041	2.5028	3.6258
	Group 5	2.5184	2.9581	1.3629	1.9583	2.3629	2.5385
	Group 6	2.3052	2.1524	2.3658	2.3147	2.5182	3.6298
	Group 7	1.3026	1.3026	2.4175	2.3528	3.6295	2.3528
	Group 8	1.5247	1.5289	1.6392	1.2518	3.6259	2.0141
	Group 9	1.6295	2.3051	1.2058	1.0241	2.1528	2.5195
	Group 10	1.3025	1.2417	1.6295	1.6295	2.6395	2.3052
RMSE		0.9258	0.2369	0.2182	0.2517	0.2147	0.2156
Average output value of test samples		2.1041	2.1427	2.9528	2.3062	2.6958	3.6285
Average evaluation result		3	3	3	4	4	4

Table 3. Incorrect prediction data of the safety level of thermodynamic disasters in deep coal mining area

Sample No. / Test group	True value	Prediction result		Description
	Safety level	Predicted value	Safety level	
Group 3	4	2.5281	3	Safe
Group 6	5	4.1027	5	Danger
Group 9	5	4.3629	6	Very danger

6. CONCLUSION

This paper studied the identification and prediction of thermodynamic disasters in deep coal mining area. At first, the paper introduced in detail the method for analyzing thermal field in deep coal mining area, and adopted finite element thermal analysis to study thermodynamic disasters during deep coal mining; then, a thermodynamic disaster prediction model was establishes based on improved KELM, and the improved CSA was introduced to solve the instability of prediction results caused by artificial selection of model parameters. Combining with experiments, this paper plotted the distribution of sampling point temperature in the deep coal mining area, gave the temperature values of the deep coal mining area in finite element numerical simulation, calculated the predicted air temperature values of the lower boundary at different ground elevations, and further attained the temperature values of the boundary within the range of the next partition spacing. Moreover, this paper designed experiments to compare the fitness of different optimization algorithms, and verified the validity of the KELM optimized by the improved CSA. At last, the verification samples, test samples, and real values were compared, and the prediction result of the safety level of thermodynamic disasters in deep coal mining area was given, which has demonstrated that the model has stable prediction performance and strong generalization ability.

REFERENCES

[1] Vorotnikov, V. (2021). Siberian coal mine disaster kills 52; exposes safety shortfalls in Russian mining industry. Engineering and Mining Journal, 222(12): 22-22.

[2] Deng, M. (2021). Feature extraction and early warning of coal mine gas disaster based on data analysis. In 2021

2nd International Conference on Artificial Intelligence and Computer Engineering (ICAICE), Hangzhou, China, pp. 421-424. 10.1109/ICAICE54393.2021.00088

[3] Wu, L., Qi, G., Lu, W., He, Z., Li, J., Li, J., He, M. (2020). Study on preparation and performance of calcium carbide slag foam for coal mine disaster reduction and CO2 storage. Colloids and Surfaces A: Physicochemical and Engineering Aspects, 606: 125322. https://doi.org/10.1016/j.colsurfa.2020.125322

[4] Lu, J., Yin, G., Gao, H., Li, X., Zhang, D., Deng, B., Li, M. (2020). True triaxial experimental study of disturbed compound dynamic disaster in deep underground coal mine. Rock Mechanics and Rock Engineering, 53(5): 2347-2364. https://doi.org/10.1007/s00603-019-02041-x

[5] Lu, J., Zhang, D., Huang, G., Li, X., Gao, H., Yin, G. (2020). Effects of loading rate on the compound dynamic disaster in deep underground coal mine under true triaxial stress. International Journal of Rock Mechanics and Mining Sciences, 134: 104453. https://doi.org/10.1016/j.ijrmms.2020.104453

[6] Lin, Z., Zhang, B., Guo, J. (2021). Analysis of a water-inrush disaster caused by coal seam subsidence karst collapse column under the action of multi-field coupling in Taoyuan coal mine. Computer Modeling in Engineering & Sciences, 126(1): 311-330. https://doi.org/10.32604/cmes.2021.011556

[7] Dai, L. (2021). Safety classification and application of coal-rock gas compound dynamic disaster in coal mine. In IOP Conference Series: Earth and Environmental Science, 651(3): 032036. https://doi.org/10.1088/1755-1315/651/3/032036

[8] Li, H, Qi, Q. Zhao, S (2021). Discussion on generalized" three factors" mechanism of coal mine dynamic disaster. Coal Science and Technology, 49(6): 42-52.

[9] Zhang, H., Han, W., Xu, Y., Wang, Z. (2021). Analysis on the development status of coal mine dust disaster prevention technology in China. Journal of Healthcare Engineering, 2021: 5574579. https://doi.org/10.1155/2021/5574579

[10] Zhao, Q., Yang, W., Hu, Q. (2021). Adaptive uneven clustering algorithm for post-disaster reconstruction of coal mine IoT. Journal of Huazhong University of Science and Technology (Natural Science Edition), 49(4): 120-126. https://doi.org/10.13245/j.hust.210421

[11] Zhou, X., Ouyang, Z., Zhou, R., Ji, Z., Yi, H., Tang, Z., Sun, B. (2021). An approach to dynamic disaster prevention in strong rock burst coal seam under multi-aquifers: A case study of tingnan coal mine. Energies, 14(21): 7287. https://doi.org/10.3390/en14217287

[12] Jiang, M., Feng, W., Gao, H., Zhang, M., Meng, X. (2021). Carbon monoxide sensor for coal mine thermodynamic disaster monitoring. Journal of the China Coal Society, 46: 793-799.

[13] Zhao, Y., Tian, S. (2021). Identification of hidden disaster causing factors in coal mine based on Naive Bayes algorithm. Journal of Intelligent & Fuzzy Systems, (Preprint), 41(2): 2823-2831. https://doi.org/10.3233/jifs-202726

[14] Wang, D. (2018). Thermodynamic disaster in coal mine and its characteristics. Journal of China Coal Society, 43(1): 137-142. https://doi.org/10.13225/j.cnki.jccs.2017.4300

[15] Zhou, A., Zhang, M., Wang, K., Elsworth, D., Wang, J., Fan, L. (2020). Airflow disturbance induced by coal mine outburst shock waves: A case study of a gas outburst disaster in China. International Journal of Rock Mechanics and Mining Sciences, 128: 104262. https://doi.org/10.1016/j.ijrmms.2020.104262

[16] Yu, M., Yang, X., Zheng, K., Luan, P. (2020). Progress and development of coal mine gas explosion suppression and disaster reduction technology in China. Journal of China Coal Society, 45: 168-188.

[17] Wen, G.C., Sun, H.T., Cao, J., Liu, Y.B., Dai, L.C., Wang, B. (2020). Simulation experiment system of coal and gas dynamic disaster in deep mine and its application in accident analysis. Journal of China Coal Society, 45(1): 223-231. https://doi.org/10.13225/j.cnki.jccs.YG19.1556

[18] Wu, T., Yang, W., Wang, Y. (2020). Self-organized energy-efficient clustering protocol for post-disaster reconstruction network of coal mine IoT. Journal of Huazhong University of Science and Technology (Natural Science Edition), 48(10): 7-13.

[19] Zhao, Q., Yang, W., Hu, Q. (2020). Adaptive clustering reconstruction algorithm of the Internet of Things after coal mine disaster. Journal of the China Coal Society, 45: 1118-1126.

[20] Xu, Y., Yang, W., Hu, Q. (2019). An autonomous discovery mechanism of surviving IoT devices for post-disaster coal mine cellular IoT. Journal of the China Coal Society, 44: 800-807.

[21] Lu, X., Kan, S. (2020). Key technology and prospect of the original source early warning method for coal mine dynamic disaster. Journal of China Coal Society, 45(S1): 128-139.

[22] Yu, X., Mu, C., Wang, H., Dou, L., Wen, H. (2022). Mining mode of layered and coordinated disaster reduction in thick coal seam of Barapukuria Coal Mine in Bangladesh. Journal of the China Coal Society, 47(6): 2352-2359.

[23] Wang, L., Chen, L., Gao, L. (2022). Warning model of coal mine ventilation disaster based on the combination of k-neighborhood-gray correlation method and its application. International Journal of Heat and Technology, 40(3): 849-854. https://doi.org/10.18280/ijht.400326

[24] Lyu, P., Lu, K., & Chen, X. (2022). Mining Stress Distribution in Stope and Overlying Rock Fracture Characteristics and Its Disaster-Pregnant Mechanism of Coal Mine Earthquake. Shock and Vibration, 2022: 7606360. https://doi.org/10.1155/2022/7606360

[25] Chen, X., Li, L., Wang, L. (2022). The mechanical effect of typical dynamic disaster evolution and occurrence in coal mines. Energy Sources, Part A: Recovery, Utilization and Environmental Effects, 44(2): 2839-2850. https://doi.org/10.1080/15567036.2019.1651792

[26] Ma, H., Wang, L., Niu, X.G., Yao, F., Zhang, K., Chang, J., Hu, Z. (2021). Mechanical characteristics of coal and rock in mining under thermal-hydraulic-mechanical coupling and dynamic disaster control. Mathematical Problems in Engineering, 2021: 9991425. https://doi.org/10.1155/2021/9991425

[27] Zhou, G., Cheng, W.M., Zhang, R., Shen, B.T., Nie, W., Zhang, L., Wang, H. (2015). Numerical simulation and disaster prevention for catastrophic fire airflow of main air-intake belt roadway in coal mine—a case study. Journal of Central South University, 22(6): 2359-2368. https://doi.org/10.1007/s11771-015-2761-x